REPORT

BRAIN MICROCIRCUITS

Layer-specific modulation of neocortical dendritic inhibition during active wakefulness

William Muñoz,[1]* Robin Tremblay,[1]* Daniel Levenstein,[1,2] Bernardo Rudy[1,3]†

γ-Aminobutyric acid (GABA)ergic inputs are strategically positioned to gate synaptic integration along the dendritic arbor of pyramidal cells. However, their spatiotemporal dynamics during behavior are poorly understood. Using an optical-tagging electrophysiological approach to record and label somatostatin-expressing (Sst) interneurons (GABAergic neurons specialized for dendritic inhibition), we discovered a layer-specific modulation of their activity in behaving mice. Sst interneuron subtypes, residing in different cortical layers and innervating complementary laminar domains, exhibited opposite activity changes during transitions to active wakefulness. The relative weight of vasoactive intestinal peptide–expressing (Vip) interneuron–mediated inhibition of distinct Sst interneurons and cholinergic modulation determined their in vivo activity. These results reveal a state-dependent laminar influence of Sst interneuron–mediated inhibition, with implications for the compartmentalized regulation of dendritic signaling in the mammalian neocortex.

Dendrites are specialized compartments for the reception, processing, and storage of the majority of incoming synaptic inputs (*1*). At the subcellular level, somatostatin-expressing (Sst) interneuron inhibitory synapses placed along the dendritic tree of a pyramidal neuron can veto synaptic integration (*2*) and Ca^{2+} electrogenesis (*3*, *4*) with fine spatiotemporal specificity (*5*). Recent studies in several neocortical areas have highlighted the participation of superficial layer 2/3 (L2/3) Sst interneurons in a canonical disinhibitory circuit supporting context-dependent sensory processing, in which the activity of L2/3 Sst interneurons is suppressed by the action of interneuron-selective vasoactive intestinal peptide–expressing (Vip) interneurons (*6*). Removing dendritic inhibition facilitates the generation of Ca^{2+} spikes and burst firing of pyramidal neurons (*7*), thereby modulating the gain of their responses as a key mechanism for sensorimotor integration (*7*–*9*), reinforcement encoding (*10*), and selective attention (*11*). However, the focus on superficial L2/3 Sst interneuron circuits in vivo, which minimally target the main input and output excitatory cells in L4 and L5/6, respectively, reflects technical limitations in accessing Sst interneurons situated deeper in the cortex, comprising both the most diverse (*12*–*14*) as well as the majority of this class of interneuron (*6*, *15*, *16*).

To investigate the contribution of the Sst interneuron population to dendritic inhibitory action during behavior, we used channelrhodopsin-assisted patching (*14*). This method gives access to the activity and morphology of targeted cells at any brain depth (Fig. 1A). Using this strategy in awake Sst^{Cre} mice (*17*) crossed to a reporter line that conditionally expresses channelrhodopsin-2 (ChR2)–enhanced yellow fluorescent protein (EYFP) (*18*), we recorded and labeled light-responsive Sst interneurons throughout all layers of the somatosensory barrel cortex (Fig. 1, A and B). To directly relate Sst interneuron activity to behavioral state, we monitored quiescence and whisking periods with whisker pad electromyogram (EMG) recordings, as well as local field potentials (LFPs) at the cortical recording site (Fig. 1A and fig. S1). Our data set consisted of 91 Sst interneurons, 50 of which were labeled and histologically analyzed (Fig. 1 and figs. S2 and S3). The laminar distribution of recorded Sst interneurons was similar to the observed distribution of immunopositive Sst neurons throughout the cortical column (Fig. 1B). In this data set, 86% of the recorded Sst interneurons exhibited significant activity modulation during whisking epochs (Fig. 1, C to F, and fig. S4). Whisking behavioral states were accompanied by transitions to neocortical network activation (as defined by decreased power of low frequencies and increased power of high frequencies in the LFP, fig. S1).

Spiking activity of all L2/3 Sst interneurons was suppressed (Wh_{OFF}) during whisking [Fig. 1, C and E to F; (*7*–*9*)]. In contrast, all modulated L4 Sst interneurons strongly increased their spiking activity (Wh_{ON}) during whisking (Fig. 1, D to F). In infragranular layers, activity was heterogeneous. Wh_{OFF} Sst interneurons were enriched in L5a, whereas the majority of the Sst interneurons in layers 5b to 6 were Wh_{ON} (Fig. 1, E and F). Wh_{ON} and Wh_{OFF} activity profiles were associated with similar whisking behavioral parameters (i.e., duration and interwhisking intervals) and LFP frequency–power representations, suggesting that these findings are not due to preparation differences (i.e., different levels of arousal between animals; fig. S1).

Sst interneurons in different cortical layers have been associated with distinct axonal distributions (*12*, *13*). We hypothesized that the laminar distribution of Wh_{ON} and Wh_{OFF} activity profiles reflected specific Sst interneuron subtypes. Thus, we analyzed the axonal projection patterns of a subset of the cells that were functionally characterized and labeled in vivo ($n = 39$ cells identified morphologically by serial-section confocal imaging, of which 22 were digitally reconstructed; Fig. 2 and fig. S5). This analysis revealed five distinct morphological subtypes (fig. S5). Wh_{ON} and Wh_{OFF} activity patterns were exclusively represented by specific subtypes, biased to cortical layers that were consistent with the laminar distribution of whisking-related activity profiles (Fig. 2 and figs. S5 and S6). L2/3 Sst interneurons were prototypical Martinotti cells with ascending axonal projections extensively innervating L1 to L3 (Fig. 2A), where they inhibit the dendrites of L2/3 pyramidal cells but target only weakly and with low probability L5 pyramidal cells (*19*, *20*). In contrast, L4 Sst interneurons, designated as non-Martinotti because of the lack of significant L1 innervation, had axons restricted to L4 (Fig. 2B), where they preferentially inhibit local parvalbumin-expressing (Pvalb) interneurons in vitro (*13*). Because L2/3 Martinotti cells are exclusively Wh_{OFF} and L4 non-Martinotti cells are Wh_{ON} (Fig. 2, A and B) and they selectively target L2/3 pyramidal cells and L4 Pvalb interneurons, respectively, the impact of their activity is predicted to result in layer-specific disinhibition during whisking (fig. S7).

Infragranular Sst interneurons with different whisking-related activity profiles were intermingled, with somatic localization biases of Wh_{OFF} cells to L5a and Wh_{ON} cells to layers 5b to 6 (Fig. 1, E and F). This intermingled distribution comprised distinct Sst interneuron subtypes with complementary, minimally overlapping axonal domains, which also acted in stereotypical Wh_{ON} or Wh_{OFF} fashion (Fig. 2, C to F, and fig. S5). In particular, infragranular Wh_{OFF} Sst interneurons in L5a and L5b were Martinotti cells with local axonal plexus in L5a and translaminar axons restricted to the uppermost part of L1 (designated "T-shaped" because of axon characteristics, Fig. 2D and fig. S5). In contrast, infragranular Wh_{ON} Martinotti Sst interneuron axons were more broadly distributed to lower L1 and L2/3 (designated "fanning-out" because of axon characteristics, Fig. 2E). Their cell bodies and local axonal domains were also located deeper than those of infragranular L5a and L5b Wh_{OFF} Martinotti cells (Fig. 2, C to E, and fig. S5). The remaining subset of infragranular L5a and L5b Wh_{ON} Sst interneurons

[1]Neuroscience Institute and Department of Neuroscience and Physiology, New York University School of Medicine, 550 First Avenue, New York, NY 10016, USA. [2]Center for Neural Science, New York University, 4 Washington Place, New York, NY 10003, USA. [3]Department of Anesthesiology, Perioperative Care and Pain Medicine, New York University School of Medicine, 550 First Avenue, New York, NY 10016, USA.
*These authors contributed equally to this work. †Corresponding author. Email: bernardo.rudy@nyumc.org

were non-Martinotti cells, with somatic localization and local axon plexus in L5b and L5b/6 and substantial innervation of L3 and L4 (Fig. 2F and fig. S5). Although the efferent connectivity of L5/6 non-Martinotti cells has not been explored, infragranular Sst Martinotti cells potently inhibit L5 pyramidal neurons (*20*, *21*). Because of the differences and complementarity in targeting domains of infragranular Sst Wh_{ON} and Wh_{OFF} Martinotti subtypes, a spatial rerouting of inhibition onto L5 pyramidal cells occurs during whisking, with increased inhibition on dendritic segments localized in L2/3 (i.e., apical and oblique dendrites) and withdrawal of inhibition on their distal tufts in the superficial part of L1. These inhibitory and disinhibitory effects predict an interplay with the laminar organization of excitatory inputs along compartments of the elaborate dendritic arbors of L5 pyramidal neurons (fig. S7).

What mechanisms contribute to the activity of distinct Sst interneurons during whisking? Vip interneurons play a crucial role in silencing L2/3 Sst interneurons (*22*) during active behavioral states (*8*–*10*). Our finding that the majority of granular and infragranular Sst interneurons are Wh_{ON} appears to be at odds with the operations of this canonical circuit. However, the strength of Vip interneuron–mediated inhibition has not been systematically evaluated across Sst interneurons of different layers or subtypes. Given that Vip interneuron axonal innervation peaks in L2/3 and L5a (*23*), we reasoned that differential Vip interneuron inhibitory inputs to Sst interneurons across layers could play a key role in the laminar distribution of whisking activity profiles in vivo. We therefore conditionally expressed ChR2 in Vip interneurons and performed voltage-clamp recordings of light-evoked inhibitory postsynaptic charges onto mCherry-expressing Sst interneurons in cortical slices from Vip^{Cre};Sst^{Flp} double-transgenic mice (Fig. 3, A and B, and fig. S8). We found stronger synaptic inputs from Vip interneurons onto L2/3 Sst interneurons than onto L4 to L6 Sst interneurons (Fig. 3B, left). The only infragranular Sst interneurons that received strong Vip interneuron inputs were located in L5a, matching the laminar-localization bias observed for infragranular Wh_{OFF} Sst interneurons. Indeed, a direct comparison of Vip interneuron–mediated inhibition on infragranular Sst interneuron subtypes yielded significantly larger light-evoked inhibitory postsynaptic charges onto T-shaped Martinotti interneurons (associated with Wh_{OFF} activity in vivo), as compared to fanning-out Martinotti and non-Martinotti cells (Fig. 3B, right). The differences in inhibitory postsynaptic charge found across Sst interneuron subtypes were strongly correlated with the number of appositions from Vip interneurons, identified using vesicular GABA transporter (VGAT) colocalization as a marker for GABAergic terminals in ChR2-EYFP-expressing Vip interneuron axons apposed to recorded Sst interneurons (fig. S9). Moreover, the distribution of Vip interneuron appositions onto L2/3 and T-shaped Martinotti cells peaked at the soma, as compared to the more distal distribution on fanning-out Martinotti and non-Martinotti cells (25 to 50 μm from soma, fig. S9).

We next tested whether Vip interneuron–mediated inhibition of L2/3 and T-shaped Martinotti cells contributed to their Wh_{OFF} activity pattern in vivo. To this end, we conditionally expressed $PSAM^{L141F}$-GlyR in Vip interneurons, a pharmacogenetic actuator that effectively dampens the excitability of these interneurons upon application

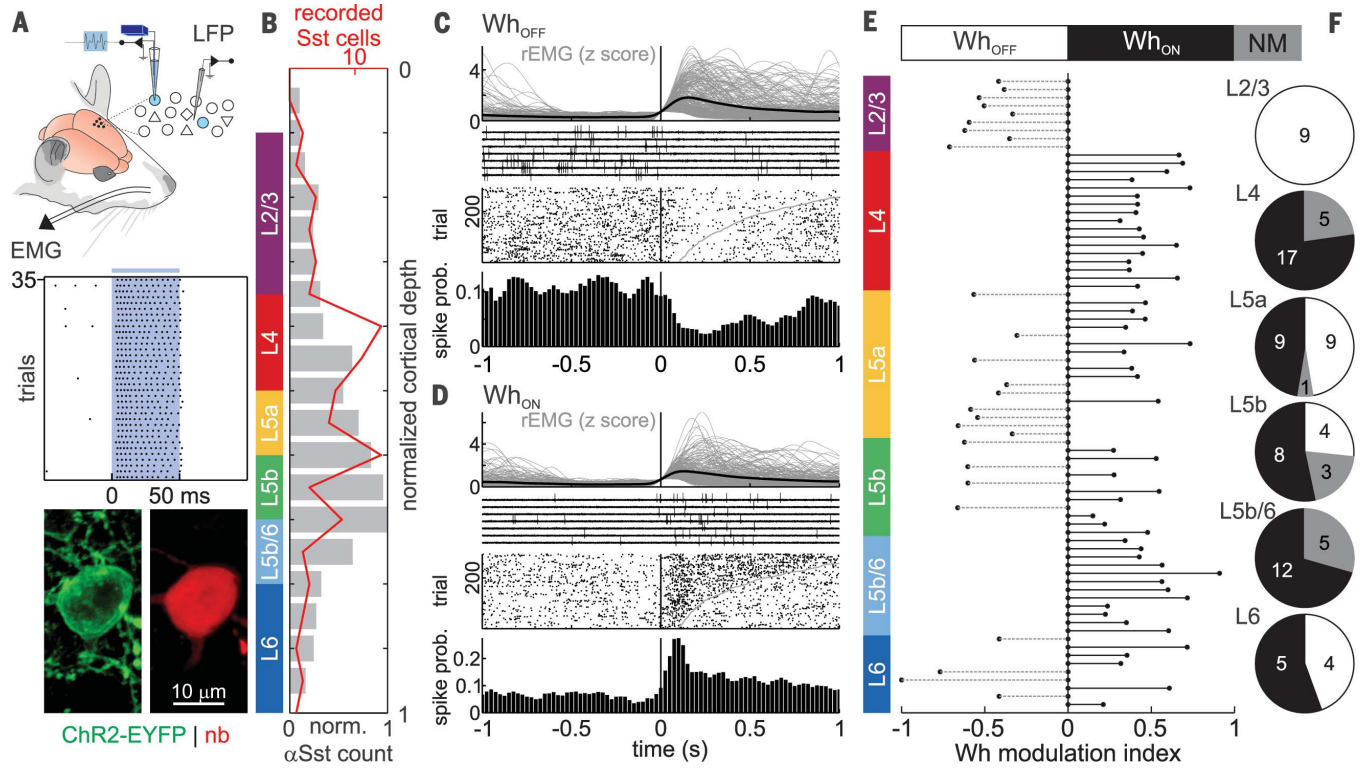

Fig. 1. Layer-specific distribution of opposite in vivo activity patterns of Sst interneurons during whisking. (**A**) (Top) Experimental setup for in vivo targeted recording of cortical Sst interneurons with channelrhodopsin-assisted patching, as well as simultaneous nearby LFP and whisker pad EMG recordings. (Middle) Raster plot of light-evoked spiking (dots) of Sst interneuron (blue area indicates light stimulus) and (Bottom) post hoc histological confirmation of ChR2-EYFP expression of this cell labeled with neurobiotin (nb). (**B**) Laminar distribution of Sst immunopositive neurons (αSst, gray bins) and of the recorded data set of Sst interneurons (red line). (**C**) Sst interneuron showing suppressed activity during whisking (Wh_{OFF}). (Top) Whisking onset–aligned rectified whisker pad EMG traces (rEMG, gray) and grand average (black). (Bottom) Normalized voltage traces of loose-patch recording (seven trials), raster plot (sorted by whisking epoch duration, gray line indicates end of bouts), and peri-event time histogram of Wh_{OFF} Sst interneuron spiking activity. (**D**) Same as (C) for an Sst interneuron increasing its spike rate during whisking (Wh_{ON}). (**E**) Whisking modulation index (see Materials and Methods) of significantly modulated Sst interneurons (sorted by cortical layer position, ranked by depth). (**F**) Proportion of Wh_{ON} (black), Wh_{OFF} (white), and nonmodulated (NM, gray) Sst interneurons in each layer. Number of cells per group is indicated in pie charts.

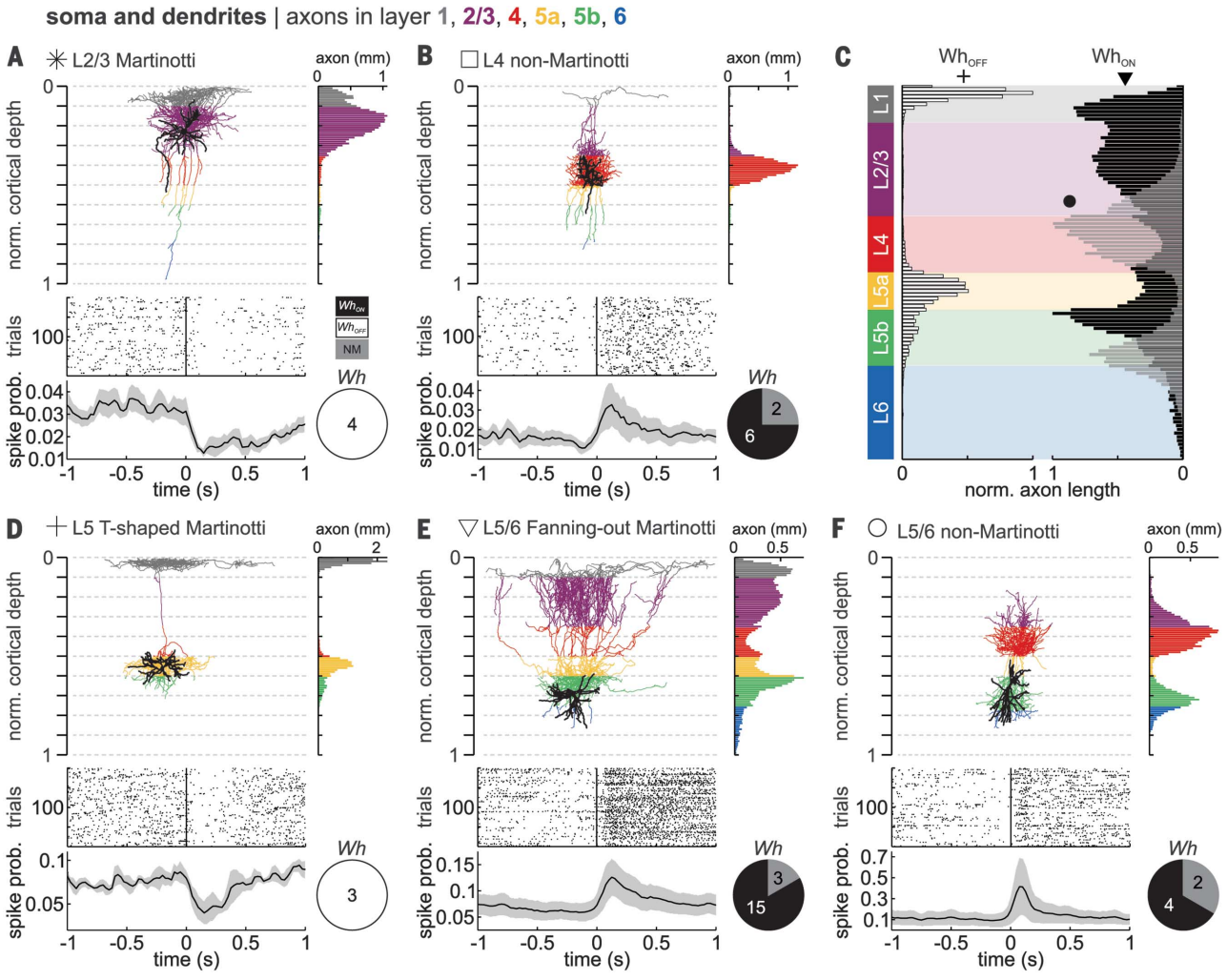

Fig. 2. Wh_{ON} and Wh_{OFF} Sst interneurons are represented by distinct subtypes with complementary axonal innervation domains. (**A**) (Top, left) Digital reconstruction of an in vivo recorded and labeled L2/3 Sst Martinotti interneuron (asterisk). Axons are color coded by layer, and somas and dendrites are black. (Top, right) Histogram shows average axonal length of reconstructed cells (n = 3 reconstructions). (Middle) Whisking onset–aligned raster plot and (bottom) population peri-event time histogram of spiking activity and proportion of whisking-related activity profiles of morphologically identified cells. Number of identified cells per activity profile is indicated in the pie chart. (**B**) Same as in (A) for L4 non-Martinotti cells (square, n = 4 reconstructions). (**C**) Complementary axonal-distribution profiles of Wh_{OFF} (left) and Wh_{ON} (right) infragranular Sst interneuron subtypes, as indicated by symbol code in (D) to (F). (**D**) Same as in (A) for L5 T-shaped Martinotti cells (cross, n = 3 reconstructions). (**E**) Same as in (A) for L5/6 fanning-out Martinotti cells (triangle, n = 7 reconstructions). (**F**) Same as in (A) for L5/6 non-Martinotti cells (circle, n = 5 reconstructions).

of its synthetic ligand PSEM^{308} [fig. S8 (*24*)]. We also conditionally expressed ChR2 in GABAergic neurons in these *Vip^{Cre};PSAM^{L141F}-GlyR* mice, using a viral vector in which ChR2 expression is under the control of the *mDlx* enhancer (*25*). This enabled in vivo channelrhodopsin-assisted patching of Sst interneurons identified by functional and histological methods (Fig. 3C and fig. S3). Suppression of Vip interneuron activity in vivo by local application of 0.5 mM PSEM^{308} released Wh_{OFF} Sst interneurons from this inhibitory source, converting their activity pattern to the Wh_{ON} phenotype (Fig. 3, C and D). However, this manipulation had no significant effect on the activity profile of Wh_{ON} Sst interneurons, confirming their weaker inhibition by Vip interneurons (Fig. 3D). These results establish a causal link between Vip interneuron–mediated inhibition and the Wh_{OFF} activity profile of Sst interneurons.

What drives the activity of Wh_{ON} Sst interneurons during whisking? Excitatory afferents to somatosensory cortex from the thalamus (*26*–*28*) and primary motor cortex (*29*) are active during whisking. However, Sst interneurons receive only weak excitation from these sources (*8*, *30*). In addition, the activity modulation of pyramidal cells in different layers is heterogeneous during whisking, and their overall laminar trends are inconsistent with Sst interneurons simply following their local network (*31*, *32*). In contrast, cholinergic activity in neocortex from basal forebrain axons is associated with both whisking and locomotion (*33*, *34*), and Sst interneurons are strongly depolarized by muscarinic receptor activation in vitro (*13*, *35*–*37*). We hypothesized that acetylcholine could be an important factor driving the activity of Sst interneurons during whisking. Thus, we examined the effect of pharmacologically blocking muscarinic receptors in vivo on the whisking activity profiles of Sst interneurons. Local application of atropine (0.5 to 1 mM) diminished, abolished, or even reversed the activity modulation of Wh_{ON} Sst interneurons and further suppressed Wh_{OFF} cells (Fig. 4, A and B). Acetylcholine has effects on multiple neocortical cell types and synapses (*38*). We next tested whether the in vivo cholinergic modulation of Wh_{ON} Sst interneurons is a cell-autonomous effect. To this end, we crossed *Sst^{Cre}* mice with *Chrm1$^{flox/flox}$* and *Chrm3$^{flox/flox}$* mouse lines to generate mice for which both M1 and M3 muscarinic receptors were genetically ablated specifically in Sst interneurons. The

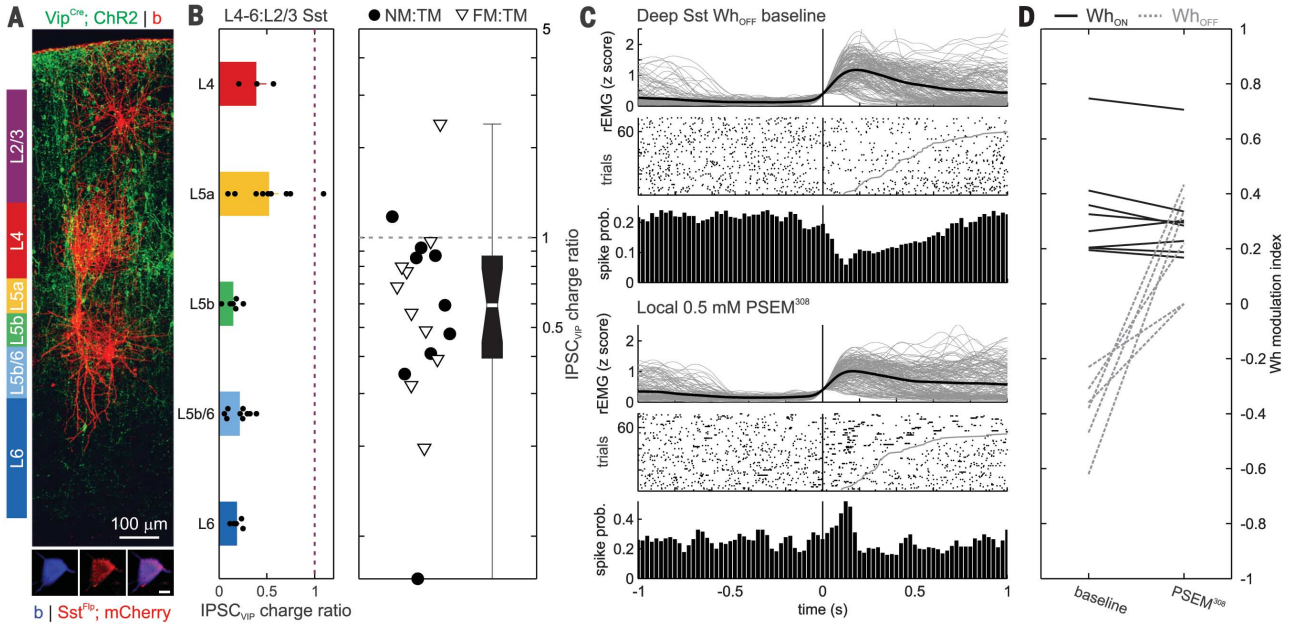

Fig. 3. Wh_{OFF} Sst interneuron activity profile is determined by stronger Vip interneuron–mediated inhibition. (**A**) (Top) Confocal image of in vitro recorded and biocytin-labeled Sst interneurons (b, red), overlaid with Vip^{Cre}; ChR2-EYFP expression profile (green). (Bottom) Confirmation of Sst^{Flp}; mCherry expression of the L2/3 Sst interneuron. (**B**) (Left) Light-evoked Vip interneuron–mediated inhibitory postsynaptic current ($IPSC_{VIP}$) charge ratio between L4 to L6 Sst interneuron recordings and their paired L2/3 Sst interneuron (compared to L2/3: L4, n = 3 pairs, $P < 0.05$; L5a, n = 9 pairs, $P < 0.01$; L5b, $n = 6$ pairs, $P < 0.001$; L5b/6, $n = 9$ pairs, $P < 0.001$; L6, $n = 5$ pairs, $P < 0.001$; paired t test). Dots indicate each pair, bars are mean and SEM, and dashed line indicates L2/3 Sst interneuron $IPSC_{VIP}$ charge level. (Right) $IPSC_{VIP}$ charge ratio between non-Martinotti (NM, circles) or fanning-out Martinotti (FM, triangles) and paired T-shaped Martinotti cell (n = 19 pairs, $P <$ 0.01, paired t test). Box plot indicates median and upper and lower quartiles, with notches as 95% confidence interval of non-Martinotti and fanning-out Martinotti charge ratios. Dashed line indicates T-shaped Martinotti $IPSC_{VIP}$ charge level. (**C**) Whisking onset–aligned rectified whisker pad EMG traces (gray) and grand average (black), raster plot (sorted by whisking epoch duration, gray line indicates end of bouts), and peri-event time histogram of an infragranular Wh_{OFF} Sst interneuron spiking activity before (top panels) and after (bottom panels) local perfusion of 0.5 mM $PSEM^{308}$. (**D**) Change in whisking modulation index following application of $PSEM^{308}$ for Wh_{OFF} (n = 6 cells, $P < 0.001$, paired t test) and Wh_{ON} ($n = 8$ cells, $P > 0.05$, paired t test) Sst interneurons.

number and laminar distribution of neocortical Sst interneurons in mutant mice and their intrinsic electrophysiological properties were similar to those in wild-type mice (fig. S10). Notably, in vitro experiments confirmed that Sst interneurons in mutant mice were insensitive to muscarine (fig. S10). We next expressed ChR2 in Sst interneurons in mutant mice to perform in vivo channelrhodopsin-assisted patching and recorded a sample of muscarinic receptor–ablated Sst interneurons in L2 to L6 (n = 17 cells). Under the same awake conditions as those used in recordings of wild-type Sst interneurons, all but one mutant Sst interneurons exhibited Wh_{OFF} activity profiles (Fig. 4, C to E). These mutant Wh_{OFF} Sst interneurons were located in layers with expected predominance of Wh_{ON} profiles (e.g., L4; Fig. 4, D and E). Our results suggest that cholinergic modulation of Sst interneurons via M1 and/or M3 muscarinic receptors provides a major excitatory drive to these cells during whisking and is a key mediator of the Wh_{ON} activity profile. Together with our findings of differential Vip interneuron–mediated inhibition to Sst interneuron subtypes, we find evidence supporting a push-pull mechanism in which inhibition and cholinergic drive weigh differently on the activity of Wh_{ON} and Wh_{OFF} Sst subtypes during whisking. In the context of our in vivo manipulations, we are able to shift the balance between these two factors, exposing their underlying influence and switching Wh_{ON} and Wh_{OFF} activity profiles in distinct Sst interneuron subtypes.

Our results thus far reveal the existence of functionally distinct Sst interneuron subtypes, which are localized in specific layers, have specialized innervation patterns, and act in opposite ways during whisking behavior. We next asked whether the functional distinction between these subtypes is also observed during quiescent or nonwhisking states. Quiet wakefulness is associated with prominent fluctuations in the power of the delta (1 to 4 Hz) and gamma (40 to 100 Hz) frequency bands of the neocortical LFP, which track rhythmic shifts in the excitability of cortical networks (*39*–*45*). We thus analyzed the relationship between the spiking of Wh_{ON} and Wh_{OFF} Sst interneurons and the power and phase of these LFP frequency bands during nonwhisking epochs. The spike rate of Wh_{ON} Sst interneurons was more strongly correlated with the power of LFP delta-band activity than that of Wh_{OFF} Sst interneurons (fig. S11). This behavior of Wh_{ON} Sst interneurons also contrasted with the weak spike rate–delta power correlation of pyramidal and Pvalb interneurons (fig. S11). Moreover, the spiking of distinct Sst interneuron subtypes was coupled to different phases of delta oscillatory cycles (fig. S12A). In addition, Sst interneuron spiking exhibited an orthogonal phase coupling to gamma oscillatory cycles with respect to that of pyramidal and Pvalb interneurons (fig. S12B). Thus, we also find traces of the division of labor between Sst interneuron subtypes during delta oscillations, and a distinct profile of Sst interneuron activity with gamma oscillations, as compared to Pvalb or pyramidal neurons during quiescent behavior.

Current understanding of the spatiotemporal action of neocortical dendritic inhibition during behavior is limited. Multiple studies performed in L2/3 from sensory and associative neocortical areas have shown that Sst interneurons are suppressed during whisking (*7*, *8*), locomotion (*9*), and different phases of learned tasks (*10*). These findings implied that pyramidal dendrites are globally disinhibited during active behavior. Here we report a layer-specific modulation of the activity of Sst interneurons, with potential circuit implications of cell type–specific disinhibition and compartmentalized inhibitory and disinhibitory effects on pyramidal cells (fig. S7). At the cellular scale, this modulation could dramatically change the reception and integration of excitatory inputs that are spatially segregated by layers (*46*, *47*), as well as their impact on the initiation sites of dendritic

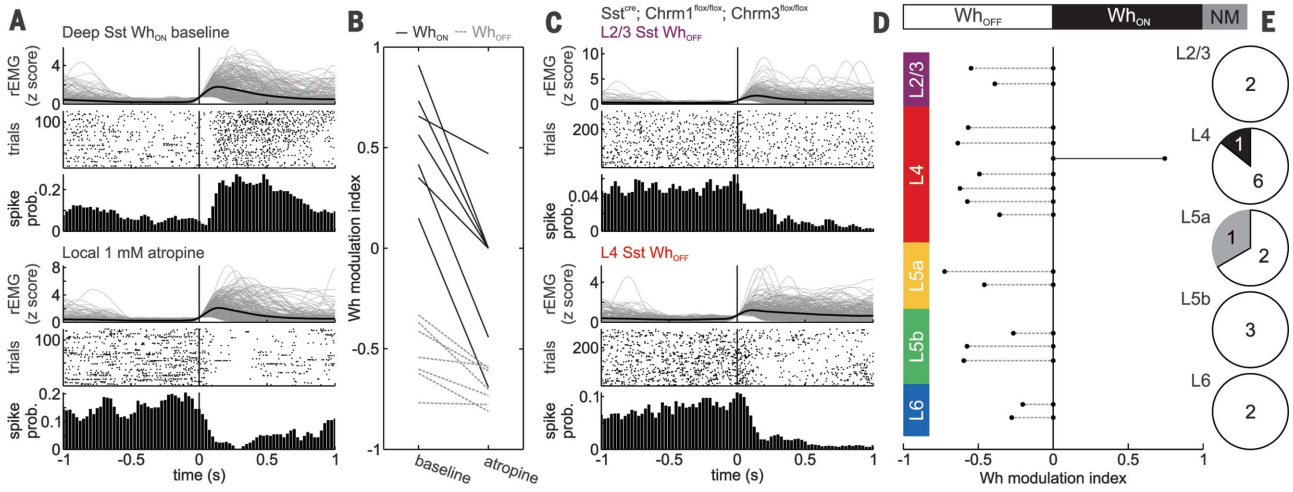

Fig. 4. Cholinergic modulation of Sst interneurons via M1 and/or M3 muscarinic receptors mediates the Wh_{ON} activity profile. (**A**) Whisking onset–aligned rectified whisker pad EMG traces (gray) and grand average (black), raster plot, and peri-event time histogram of infragranular Wh_{ON} Sst interneuron spiking activity before (top panels) and after (bottom panels) local perfusion of 1 mM atropine. (**B**) Change in whisking modulation index following application of atropine for Wh_{ON} ($n = 7$ cells, $P < 0.01$, paired t test) and Wh_{OFF} ($n = 7$ cells, $P < 0.05$, paired t test) Sst interneurons. (**C**) Whisking-related activity of Wh_{OFF} L2/3 (top) and L4 (bottom) M1 and M3 muscarinic receptor–ablated Sst interneurons in Sst^{Cre};$Chrm1^{flox/flox}$; $Chrm3^{flox/flox}$ mice. Panels are displayed as in (A). (**D**) Whisking modulation index of significantly modulated M1 and M3 muscarinic receptor–ablated Sst interneurons (sorted by cortical layer position, ranked by depth). (**E**) Proportion of whisking-related activity profiles in each layer. Number of cells per group is indicated in the pie charts.

N-methyl-D-aspartate (NMDA) and Ca^{2+} spikes [fig. S7 (*48*)]. At the network scale, the processing of associative and sensory signals in L2/3 and L4, respectively, might be strengthened because of Sst interneuron–mediated disinhibition of excitatory neurons, whereas operations in L5, the main cortical output layer, might be subject to more refined compartmentalized inhibitory regulation (fig. S7). Future experiments addressing the molecular identity of morphologically identified Sst interneuron subtypes will enable manipulation and causal testing of their function in neocortical circuits (*6*). Understanding their connectivity principles will improve our conceptual frameworks of how dendritic inhibition gates neuronal and network excitability. Additional work is needed to examine the extent and dynamics with which neocortical networks exploit these functionally distinct sources of dendritic inhibition in the context of cognitive processes, such as attention and learning.

REFERENCES AND NOTES

1. N. Spruston, *Nat. Rev. Neurosci.* **9**, 206–221 (2008).
2. C. Q. Chiu *et al.*, *Science* **340**, 759–762 (2013).
3. M. E. Larkum, J. J. Zhu, B. Sakmann, *Nature* **398**, 338–341 (1999).
4. M. Murayama *et al.*, *Nature* **457**, 1137–1141 (2009).
5. F. E. Müllner, C. J. Wierenga, T. Bonhoeffer, *Neuron* **87**, 576–589 (2015).
6. R. Tremblay, S. Lee, B. Rudy, *Neuron* **91**, 260–292 (2016).
7. L. J. Gentet *et al.*, *Nat. Neurosci.* **15**, 607–612 (2012).
8. S. Lee, I. Kruglikov, Z. J. Huang, G. Fishell, B. Rudy, *Nat. Neurosci.* **16**, 1662–1670 (2013).
9. Y. Fu *et al.*, *Cell* **156**, 1139–1152 (2014).
10. H. J. Pi *et al.*, *Nature* **503**, 521–524 (2013).
11. S. Zhang *et al.*, *Science* **345**, 660–665 (2014).
12. Y. Ma, H. Hu, A. S. Berrebi, P. H. Mathers, A. Agmon, *J. Neurosci.* **26**, 5069–5082 (2006).
13. H. Xu, H. Y. Jeong, R. Tremblay, B. Rudy, *Neuron* **77**, 155–167 (2013).
14. W. Muñoz, R. Tremblay, B. Rudy, *Cell Rep.* **9**, 2304–2316 (2014).
15. S. Lee, J. Hjerling-Leffler, E. Zagha, G. Fishell, B. Rudy, *J. Neurosci.* **30**, 16796–16808 (2010).
16. X. Xu, K. D. Roby, E. M. Callaway, *J. Comp. Neurol.* **518**, 389–404 (2010).
17. H. Taniguchi *et al.*, *Neuron* **71**, 995–1013 (2011).
18. L. Madisen *et al.*, *Nat. Neurosci.* **15**, 793–802 (2012).
19. X. Jiang, G. Wang, A. J. Lee, R. L. Stornetta, J. J. Zhu, *Nat. Neurosci.* **16**, 210–218 (2013).
20. X. Jiang *et al.*, *Science* **350**, aac9462 (2015).
21. G. Silberberg, H. Markram, *Neuron* **53**, 735–746 (2007).
22. C. K. Pfeffer, M. Xue, M. He, Z. J. Huang, M. Scanziani, *Nat. Neurosci.* **16**, 1068–1076 (2013).
23. A. Prönneke *et al.*, *Cereb. Cortex* **25**, 4854–4868 (2015).
24. C. J. Magnus *et al.*, *Science* **333**, 1292–1296 (2011).
25. J. Dimidschstein *et al.*, *Nat. Neurosci.* **19**, 1743–1749 (2016).
26. J. F. Poulet, L. M. Fernandez, S. Crochet, C. C. Petersen, *Nat. Neurosci.* **15**, 370–372 (2012).
27. N. Urbain *et al.*, *Cell Rep.* **13**, 647–656 (2015).
28. J. Yu, D. A. Gutnisky, S. A. Hires, K. Svoboda, *Nat. Neurosci.* **19**, 1647–1657 (2016).
29. L. Petreanu *et al.*, *Nature* **489**, 299–303 (2012).
30. S. J. Cruikshank, H. Urabe, A. V. Nurmikko, B. W. Connors, *Neuron* **65**, 230–245 (2010).
31. C. P. de Kock, B. Sakmann, *Proc. Natl. Acad. Sci. U.S.A.* **106**, 16446–16450 (2009).
32. D. H. O'Connor, S. P. Peron, D. Huber, K. Svoboda, *Neuron* **67**, 1048–1061 (2010).
33. E. Eggermann, Y. Kremer, S. Crochet, C. C. Petersen, *Cell Rep.* **9**, 1654–1660 (2014).
34. A. Nelson, R. Mooney, *Neuron* **90**, 635–648 (2016).
35. Y. Kawaguchi, *J. Neurophysiol.* **78**, 1743–1747 (1997).
36. M. Beierlein, J. R. Gibson, B. W. Connors, *Nat. Neurosci.* **3**, 904–910 (2000).
37. N. Chen, H. Sugihara, M. Sur, *Nat. Neurosci.* **18**, 892–902 (2015).
38. W. Muñoz, B. Rudy, *Curr. Opin. Neurobiol.* **26**, 149–160 (2014).
39. S. Crochet, C. C. Petersen, *Nat. Neurosci.* **9**, 608–610 (2006).
40. P. Lakatos, G. Karmos, A. D. Mehta, I. Ulbert, C. E. Schroeder, *Science* **320**, 110–113 (2008).
41. K. D. Harris, A. Thiele, *Nat. Rev. Neurosci.* **12**, 509–523 (2011).
42. G. Buzsáki, X. J. Wang, *Annu. Rev. Neurosci.* **35**, 203–225 (2012).
43. G. Buzsáki, C. A. Anastassiou, C. Koch, *Nat. Rev. Neurosci.* **13**, 407–420 (2012).
44. M. J. McGinley, S. V. David, D. A. McCormick, *Neuron* **87**, 179–192 (2015).
45. M. J. McGinley *et al.*, *Neuron* **87**, 1143–1161 (2015).
46. L. Petreanu, T. Mao, S. M. Sternson, K. Svoboda, *Nature* **457**, 1142–1145 (2009).
47. M. Larkum, *Trends Neurosci.* **36**, 141–151 (2013).
48. M. E. Larkum, T. Nevian, M. Sandler, A. Polsky, J. Schiller, *Science* **325**, 756–760 (2009).

ACKNOWLEDGMENTS

We are grateful to G. Buzsáki, G. Fishell, R. Froemke, W. Gan, R. Hardstone, I. Kruglikov, K. Kuchibhotla, S. Lee, M. Long, and M. Nigro for helpful discussions and comments on the manuscript. We are also grateful to Y. Hashikawa for assistance with histological analyses. Key reagents were provided by S. Tonegawa (*Chrm1*-conditional mice), J. Wess (*Chrm3*-conditional mice), J. Dimidschstein and G. Fishell (AAV-mDlx-ChR2 virus), J. Basu and S. Sternson (AAV-DIO-PSAM^{L141F}-GlyR virus), and Z. J. Huang (AAV-fDIO-mCherry virus). *Chrm1*-conditional mice are available from S. Tonegawa under a material transfer agreement with the Massachusetts Institute of Technology. *Chrm3*-conditional mice are available from J. Wess under a material transfer agreement with the National Institute of Diabetes and Digestive and Kidney Diseases. This work was supported by NIH grants R01NS30989, R21NS093987, and P01NS074972 to B.R.; National Research Service Award (NRSA) fellowship F31NS087919 to W.M.; and a Graduate Research Fellowship to R.T. from the Natural Sciences and Engineering Research Council of Canada (NSERC). Electrophysiological and histological data in this manuscript are stored in the laboratory computers. MATLAB-based data processing codes can be accessed online (https://github.com/dlevenstein/DLevenstein-Code).

SUPPLEMENTARY MATERIALS

www.sciencemag.org/content/355/6328/954/suppl/DC1
Materials and Methods
Figs. S1 to S12
References (*49*–*63*)

31 May 2016; accepted 6 February 2017
10.1126/science.aag2599

Science

Layer-specific modulation of neocortical dendritic inhibition during active wakefulness

William Muñoz, Robin Tremblay, Daniel Levenstein and Bernardo Rudy

Science **355** (6328), 954-959.
DOI: 10.1126/science.aag2599

Layer-specific interneuron activity

Somatostatin-expressing interneurons are an important group of inhibitory neurons in the brain that target and thus control the dendrites of pyramidal cells. These interneurons have recently been shown to play a role in sensorimotor integration, reinforcement encoding, and selective attention. Muñoz *et al.* used channelrhodopsin-assisted patching to investigate the spatiotemporal pattern of neocortical dendritic inhibition in vivo. They were able to record the activity of somatostatin-expressing interneurons in all neocortical layers in behaving mice. The results provide a framework for understanding the changes in dendritic inhibition that take place in the neocortex during active behaviors. This framework is very distinct from the view obtained from previous recordings that were restricted to interneurons in the superficial layers of the neocortex.

Science, this issue p. 954